The MITC9 *shell* element in *plate* bending: mathematical analysis of a simplified case

Klaus-Jürgen Bathe[1], *Franco Brezzi*[2,3], *L. Donatella Marini*[4,2]

Abstract

We consider the 9-node shell element referred to as the MITC9 *shell* element in *plate* bending solutions and present a simplified mathematical analysis. The element uses bi-quadratic interpolations of the rotations and transverse displacement, and the "rotated Raviart-Thomas" interpolations for the transverse shear stresses. A rigorous mathematical analysis of the element is still lacking, even for the simplified case of plate solutions (that is, flat shells), although the numerical evidence suggests a good and reliable behavior. Here we start such an analysis by considering a very simple particular case; namely, a rectangular plate, clamped all around the boundary, and solved with a uniform decomposition. Moreover, we consider only the so-called *limit case*, corresponding to the limit equations that are obtained for the thickness t going to zero. While the mathematical analysis of the limit case is simpler, such analysis, in general, gives an excellent indication of whether shear locking is present in the real case $t > 0$. We detail that the element in the setting considered shows indeed optimal behavior.

1 Introduction

Numerous finite elements based on Kirchhoff plate theory and Reissner-Mindlin plate theory have been proposed for linear plate analyses, see for example [1, 2]. Today, plate bending elements are available that have been proven to be optimal by mathematical

[1]MIT, Department of Mechanical Engineering, Massachusetts Institute of Technology, Cambridge, MA 02139 USA

[2]IMATI del CNR, Via Ferrata 5/A, 27100 Pavia, Italy

[3]IUSS, Lungoticino Sforza 56, 27100 Pavia, Italy

[4]Dipartimento di Matematica, Università di Pavia, Via Ferrata 5/A, 27100 Pavia, Italy

analysis and have revealed that optimal behavior also in numerical solutions, see e.g. [3]–[6]. Although these elements are available, of course, there is still important research in the analysis of plates to establish computationally more cost-effective schemes in general, and in particular for composite plate analyses where three-dimensional effects can be important.

The situation is quite different in the analysis of shells [7, 8]. Such structures are much more difficult to analyze and efficient, reliable, and generally applicable shell elements are much more difficult to develop. Indeed, while many shell elements have been proposed, there is still no element available that has been proven mathematically to always perform optimally in all shell analyses and in any mesh used. The reason is that the behavior of shell structures is greatly affected by the curvature of the shell, the boundary conditions, the thickness, and the loading applied [7]–[10]. Moreover, the *limit behaviour* of a shell for the thickness going to zero can show, even in quite realistic cases, a discouraging variety of patterns that make a unified analysis extremely difficult, see e.g. [11]–[15]. While complete convergence proofs are very difficult to achieve, and indeed still out of reach, it is important to recognize that mathematical analysis has been extremely valuable to establish discriminating numerical tests with error norms to identify the value of a shell solution scheme [8, 16, 17].

A simple shell in bending is of course a flat plate, and in practical finite element analyses it is common practice to use shell elements for plate solutions [1, 2, 18, 19, 20]. There are at least two reasons. First, in practice, plates are frequently encountered in complex structures, like in facetted configurations, with beams to act as stiffeners, or with attached cables (e.g. in a suspension bridge). In these cases, the membrane in-plane actions, like in a general shell, are very important. Second, if an originally flat plate undergoes large displacements, a full shell behavior is encountered. Hence, if an originally flat thin structure has been modeled using shell elements, a large displacement analysis can directly be pursued with the same finite element model. Therefore, ideally, we would have general shell elements that for plate bending analyses show optimal behavior, just like the optimal plate elements referred to above.

Based on these thoughts, the quadratic MITC shell elements were tested for their behavior in plate analyses [21]. Specifically, the numerical performance of the MITC shell elements, developed for general shell analyses, was compared with the performance of the MITC plate elements, designed for the linear analysis of plates and known to yield optimal solutions. An interesting conclusion was that the MITC9 shell element of ref. [22], based on the earlier element given in ref. [23], performed as well as the MITC9 plate element of refs. [3, 5]. We show these results in Figures 1.1 and 1.2. However, whereas the plate element has a strong mathematical foundation, the shell element was proposed based only on physical insight, mathematical conditions, and numerical experiments. A

mathematical analysis of this element in complex shell analyses was out of reach.

Clearly, a general mathematical analysis of the MITC9 shell element would be extremely valuable. However, it is already an important step to mathematically analyze the element when considering plate bending solutions only. Our objective in this paper is to detail such an analysis. We use a simplified setting to focus on the basic behavior of the element. The mathematical analysis shows that the convergence of the element is indeed optimal – hence, that the numerical results in ref. [21] should be expected.

The given analysis and results are valuable because the mathematical proofs give strength to the numerical findings, and the analysis yields insight that may provide a basis for more comprehensive mathematical studies of the element, also directed to the solution of complex shell structures.

In the paper, we will use the notation $A \lesssim B$ whenever there exists a constant C, depending only on the ratio of the two edges of the rectangular domain, such that $A \leq C\,B$. Clearly $A \gtrsim B$ will be used whenever $B \lesssim A$.

Throughout the paper, for s integer we will denote by $H^s(\Omega)$ the usual Sobolev space of functions that are square-integrable in Ω together with their (weak) derivatives up to the order s. We denote by $H^s_0(\Omega)$ the subspace of $H^s(\Omega)$ made of functions that vanish at the boundary $\partial\Omega$ of Ω together with all their derivatives up to the order $s-1$. Moreover $\|\cdot\|_{s,\Omega}$ or simply $\|\cdot\|_s$ will be used to indicate the usual Sobolev norm in $H^s(\Omega)$ (or copies of it). In particular we shall use the notation $\|\cdot\|_0$ and $(\cdot\,,\,\cdot)_0$ for the norm and the scalar product (respectively) in $L^2(\Omega)$ or copies of it.

2 Formulation of the problem and basic notation

In this section we formulate the continuous problem and introduce some required notation for our analysis.

2.1 The continuous problem

Let Ω be the rectangle $]0, L_1[\times]0, L_2[$. Without loss of generality we can assume that $L_1 \leq L_2$. Introducing the spaces

$$\boldsymbol{\Theta} := (H^1_0(\Omega))^2, \qquad W := H^1_0(\Omega), \tag{2.1}$$

corresponding to hard clamped boundary conditions (see, e.g., [1]), we set

$$\mathcal{U} := \boldsymbol{\Theta} \times W \tag{2.2}$$

with the norm

$$\|V\|^2_{\mathcal{U}} := \|\boldsymbol{\eta}\|^2_{1,\Omega} + \|v\|^2_{1,\Omega} \qquad \text{for } V = (\boldsymbol{\eta}, v) \in \mathcal{U}. \tag{2.3}$$

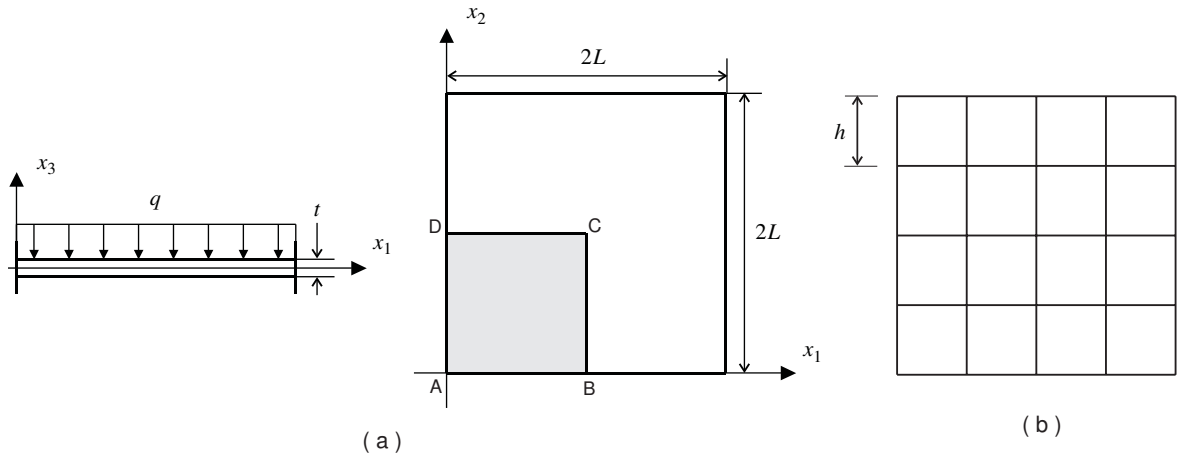

Figure 1.1: Clamped plate considered and finite element results obtained using the MITC9 shell element. (a) Square plate problem solved, uniform pressure is applied, $L_1 = L_2 = L = 1.0$, Young's modulus $= 1.7472 \times 10^7$, Poisson's ratio $= 0.30$. (b) Typical mesh used for region A-B-C-D, N=4.

We also define, for $\boldsymbol{\eta} \in \boldsymbol{\Theta}$, the symmetric gradient $\boldsymbol{\varepsilon}(\boldsymbol{\eta})$

$$(\varepsilon(\boldsymbol{\eta}))_{i,j} := \frac{1}{2}\Big(\frac{\partial \boldsymbol{\eta}_i}{\partial x_j} + \frac{\partial \boldsymbol{\eta}_j}{\partial x_i}\Big), \tag{2.4}$$

and for every $t > 0$ we define the bilinear form $\mathcal{A}_t$ on $\mathcal{U} \times \mathcal{U}$, with Young's modulus equal to 12 and Poisson's ratio equal to 0, as

$$\mathcal{A}_t(U, V) := (\boldsymbol{\varepsilon}(\boldsymbol{\theta}), \boldsymbol{\varepsilon}(\boldsymbol{\eta}))_0 + 6t^{-2}(\nabla w - \boldsymbol{\theta}, \nabla v - \boldsymbol{\eta})_0 \tag{2.5}$$

for $U = (\boldsymbol{\theta}, w)$ and $V = (\boldsymbol{\eta}, v)$. We are interested in the case "t small". Hence, even when it is not explicitly specified, we will always consider the case of t being small, certainly $t < L_1$.

The *bending part* of the bilinear form $\mathcal{A}_t$ will be usually denoted by $\mathcal{A}_b$, that is

$$\mathcal{A}_b(U, V) := (\boldsymbol{\varepsilon}(\boldsymbol{\theta}), \boldsymbol{\varepsilon}(\boldsymbol{\eta}))_0. \tag{2.6}$$

We recall the following well known result (see, e.g., [4, 8]).

Proposition 2.1. *The bilinear form $\mathcal{A}_t$ is continuous and elliptic on $\mathcal{U} \times \mathcal{U}$ for every $t > 0$, in the sense that: for every t with $0 < t < L_1$ there exist three positive constants C_t, C_b and C_s such that*

$$\mathcal{A}_t(U, V) \le C_t \, \|U\|_{\mathcal{U}} \, \|V\|_{\mathcal{U}} \qquad \forall\, U,\, V \in \mathcal{U} \tag{2.7}$$

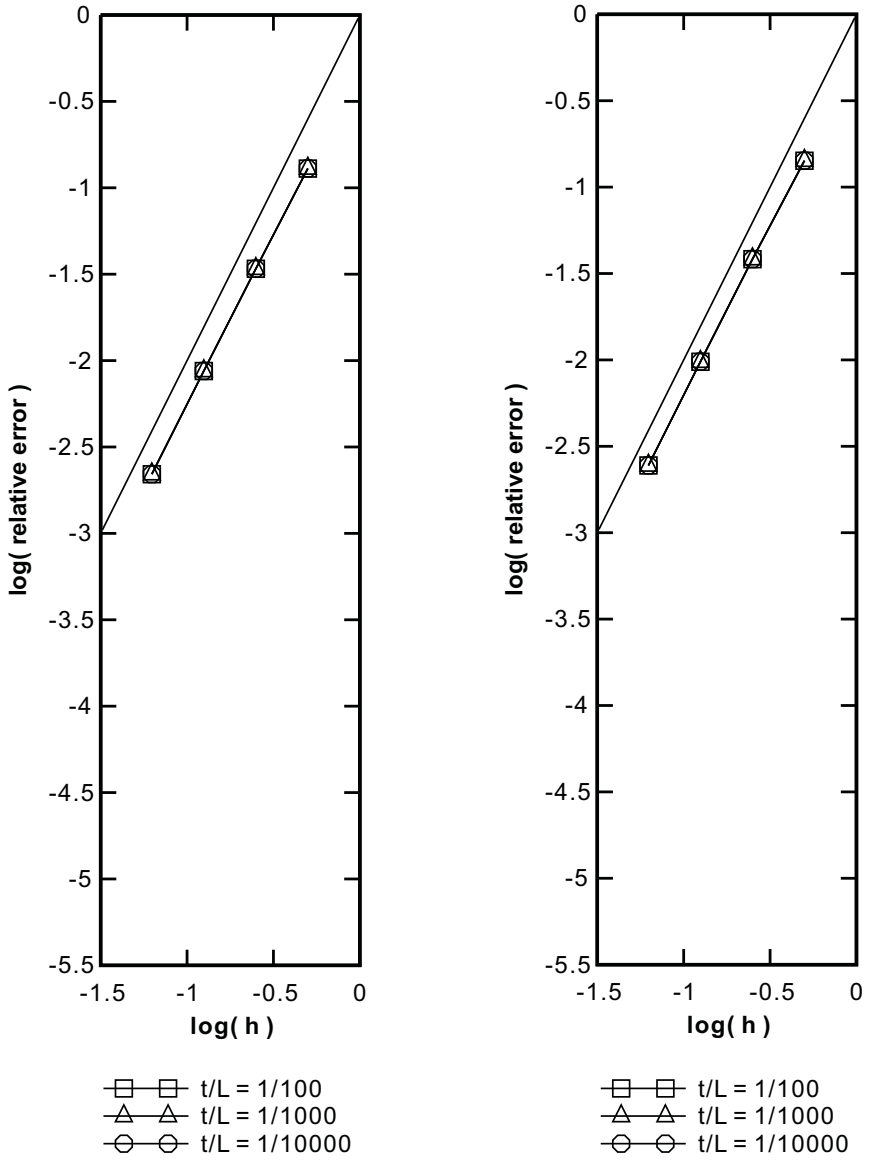

Figure 1.2: Results obtained for the clamped plate using the MITC9 shell element. Left: relative error for rotations in the H^1 norm. Right: relative error for transverse displacement in the H^1 norm. In both cases the slope is 2, as expected.

$$\mathcal{A}_b(U,V) \le C_b \|U\|_{\mathcal{U}} \|V\|_{\mathcal{U}} \qquad \forall\, U,\, V \in \mathcal{U} \tag{2.8}$$

$$\mathcal{A}_t(V,V) \ge C_s \|V\|^2_{\mathcal{U}} \qquad \forall\, V \in \mathcal{U}. \tag{2.9}$$

Moreover C_b and C_s are independent of t.

Proof. Continuity equations (2.7) and (2.8) are obvious. Next, we recall the Korn inequality: for $V = (\boldsymbol{\eta}, v) \in \mathcal{U}$

$$\mathcal{A}_b(V,V) \equiv (\boldsymbol{\varepsilon}(\boldsymbol{\eta}), \boldsymbol{\varepsilon}(\boldsymbol{\eta}))_0 \gtrsim \|\boldsymbol{\eta}\|^2_{1,\Omega}, \tag{2.10}$$

which implies

$$\mathcal{A}_t(V,V) \ge \mathcal{A}_b(V,V) \gtrsim \|\boldsymbol{\eta}\|^2_{1,\Omega}, \tag{2.11}$$

and since $L_1 > t > 0$ we obviously have

$$\|\nabla v\|^2_{0,\Omega} \le 2\|\nabla v - \boldsymbol{\eta}\|^2_{0,\Omega} + 2\|\boldsymbol{\eta}\|^2_{0,\Omega} \lesssim \mathcal{A}_t(V,V), \tag{2.12}$$

and the result follows from (2.11) and (2.12). □

Remark 2.2. *For simplicity we assumed in* (2.5) *Poisson's ratio equal to 0. However, it is clear that the properties of $\mathcal{A}_t$ and $\mathcal{A}_b$ in the above proposition (which we use for all our estimates) do not depend on this assumption.*

□

We now fix a function (load) $g \in L^2(\Omega)$ and define

$$(G,V)_0 := (g,v)_0 \qquad \text{for } V = (\boldsymbol{\eta}, v), \tag{2.13}$$

and we note that, obviously,

$$|(G,V)_0| \le \|g\|_0 \|V\|_{\mathcal{U}}. \tag{2.14}$$

We then consider the problem:

$$\begin{cases} \text{Find } U \in \mathcal{U} \text{ such that} \\ \mathcal{A}_t(U,V) = (G,V)_0 \qquad \forall V \in \mathcal{U}. \end{cases} \tag{2.15}$$

From Proposition 2.1 we have immediately existence and uniqueness of the solution of (2.15).

Proposition 2.3. *For every $t > 0$ and for every $g \in L^2(\Omega)$ problem* (2.15) *has a unique solution U that satisfies*

$$\|U\|_{\mathcal{U}} \lesssim \|g\|_0. \tag{2.16}$$

Moreover, U coincides with the unique minimizer on $\mathcal{U}$ of the functional

$$J_t^{RM}(V) := \frac{1}{2}\mathcal{A}_t(V,V) - (G,V)_0. \tag{2.17}$$

□

2.2 The Lagrange multipliers formulation

We introduce now the formulation with multipliers. For this we need to define the spaces

$$H(\mathrm{rot};\Omega) := \{\boldsymbol{\delta} \in (L^2(\Omega))^2, \text{ such that } \mathrm{rot}\boldsymbol{\delta} \in L^2(\Omega)\}, \tag{2.18}$$

where $\mathrm{rot}\boldsymbol{\delta}$, as usual in two-dimensional settings, is defined as $\mathrm{rot}\boldsymbol{\delta} := \frac{\partial \delta_2}{\partial x_1} - \frac{\partial \delta_1}{\partial x_2}$, and

$$Q := H_0(\mathrm{rot};\Omega) \equiv \{\boldsymbol{\delta} \in H(\mathrm{rot};\Omega) \text{ such that}, \boldsymbol{\delta}\cdot\mathbf{t} = 0 \text{ on } \partial\Omega\} \tag{2.19}$$

where $\mathbf{t}$ is the unit counterclockwise tangent vector to $\partial\Omega$. We also define the norm

$$\|\boldsymbol{\delta}\|_Q^2 := \|\boldsymbol{\delta}\|_{0,\Omega}^2 + \|\mathrm{rot}\boldsymbol{\delta}\|_{0,\Omega}^2. \tag{2.20}$$

We can also define the space of multipliers $\mathcal{M}$ as

$$\mathcal{M} := Q' \tag{2.21}$$

(that is, the dual space of Q). We shall often use the following notation

$$\mathcal{L} := \left(L^2(\Omega)\right)^2 \tag{2.22}$$

It is evident that $Q \subseteq \mathcal{L}$ with continuous dense embedding so that $\mathcal{L}$ (that we identify as usual with its own dual space) can be identified with a dense subspace of $\mathcal{M} = Q'$.

Remark 2.4. *It can be proved (see, e.g., [4]) that*

$$\mathcal{M} \equiv \{\boldsymbol{\mu} \in (H^{-1}(\Omega))^2 \text{ such that } \mathrm{div}\boldsymbol{\mu} \in H^{-1}(\Omega)\}. \tag{2.23}$$

□

It will also be convenient to introduce the operator $B : \mathcal{U} \to Q$ defined as

$$B(V) = \nabla v - \boldsymbol{\eta} \qquad \text{for } V = (\boldsymbol{\eta}, v). \tag{2.24}$$

The following result is well known (see e.g. [4]).

Proposition 2.5. *The space Q coincides with the image of $\mathcal{U}$ through the operator B. Moreover, for every $\boldsymbol{\delta} \in Q$ there exists a $V \in \mathcal{U}$ such that $B(V) = \boldsymbol{\delta}$ and*

$$\|V\|_{\mathcal{U}} \lesssim \|\boldsymbol{\delta}\|_Q. \tag{2.25}$$

□

We consider now the saddle-point problem:

$$\begin{cases} \text{Find } U \equiv (\boldsymbol{\theta}, w) \in \mathcal{U} \text{ and } \boldsymbol{\lambda} \in \mathcal{L} \text{ such that} \\ \mathcal{A}_b(U,V) + {}_{\mathcal{M}}{<}\boldsymbol{\lambda}, B(V){>}_{Q} = (G,V)_0 \quad \forall V \in \mathcal{U} \\ {}_{\mathcal{M}}{<}\boldsymbol{\mu}, B(U){>}_{Q} - \dfrac{t^2}{6}(\boldsymbol{\lambda},\boldsymbol{\mu})_0 = 0 \quad \forall \boldsymbol{\mu} \in \mathcal{L}. \end{cases} \tag{2.26}$$

As Proposition 2.5 implies the *inf-sup* condition

$$\exists \beta > 0 \text{ such that } \inf_{\boldsymbol{\mu}\in\mathcal{M}} \sup_{V\in\mathcal{U}} \frac{{}_{Q}{<}B(V), \boldsymbol{\mu}{>}_{\mathcal{M}}}{\|V\|_{\mathcal{U}}\,\|\boldsymbol{\mu}\|_{\mathcal{M}}} \geq \beta \tag{2.27}$$

we can easily have the following result.

Proposition 2.6. *For every $t > 0$ and for every $g \in L^2(\Omega)$, problem* (2.26) *has a unique solution $(U, \boldsymbol{\lambda})$ that satisfies*

$$\|U\|_{\mathcal{U}} + \|\boldsymbol{\lambda}\|_{\mathcal{M}} \lesssim \|g\|_0. \tag{2.28}$$

Moreover, U coincides with the solution of (2.15). □

Proof. The result is rather classical, but we summarize the proof for the convenience of the reader. Let us first consider, for every $t > 0$, the solution U of (2.15), and set $\boldsymbol{\lambda} := 6t^{-2}B(U)$ that belongs to $Q \subset \mathcal{L}$. It is easy to see that the pair $(U, \boldsymbol{\lambda})$ is a solution of (2.26). Moreover the first part of (2.28), that is

$$\|U\|_{\mathcal{U}} \lesssim \|g\|_0, \tag{2.29}$$

holds true due to (2.16). Finally, from (2.27) we immediately have that

$$\exists\, V^* \in \mathcal{U} \text{ such that } \|\boldsymbol{\lambda}\|_{\mathcal{M}} \leq \frac{1}{\beta} \frac{{}_{Q}{<}B(V^*), \boldsymbol{\lambda}{>}_{\mathcal{M}}}{\|V^*\|_{\mathcal{U}}}, \tag{2.30}$$

and using the first equation of (2.26) with $V = V^*$, and then (2.14) and (2.8), we have

$$\|\boldsymbol{\lambda}\|_{\mathcal{M}} \leq \frac{1}{\beta}\, \frac{(G,V^*)_0 - \mathcal{A}_b(U,V^*)}{\|V^*\|_{\mathcal{U}}} \lesssim (\|g\|_0 + \|U\|_{\mathcal{U}}), \tag{2.31}$$

and the result follows from (2.29) and (2.31). □

Remark 2.7. *In mathematical terms, problem* (2.26) *is* singularly perturbed*, since, for a general $G \in \mathcal{U}'$ and a general Lipschitz domain, its solution $(U(t), \boldsymbol{\lambda}(t))$ exists in $\mathcal{U} \times \mathcal{L}$ for every $t > 0$, but is* **not** *uniformly bounded in $\mathcal{U} \times \mathcal{L}$. However, $U(t)$ is uniformly bounded in $\mathcal{U}$, and the inf-sup condition* (2.27) *provides a uniform bound for $\boldsymbol{\lambda}(t)$ in $\mathcal{M}$ (although not in $\mathcal{L}$).*

2.3 The limit problem

As the bound in (2.28) does not depend on t (and $\mathcal{U}$ and $\mathcal{M}$ are Hilbert spaces), it is easy to see and well known (see e.g. [4], Theorem VII.3.1) that $U = U(t)$ and $\boldsymbol{\lambda} = \boldsymbol{\lambda}(t)$ have a limit for $t \to 0$.

Proposition 2.8. *For every $g \in L^2(\Omega)$ we have*

$$\lim_{t\to 0}(U(t), \boldsymbol{\lambda}(t)) = (U_0, \lambda_0) \tag{2.32}$$

where (U_0, λ_0) is the unique solution of the **limit problem**

$$\begin{cases} \text{Find } U_0 \equiv (\boldsymbol{\theta}_0, w_0) \in \mathcal{U} \text{ and } \boldsymbol{\lambda}_0 \in \mathcal{M} \text{ such that} \\ \mathcal{A}_b(U_0, V) + {}_{\mathcal{M}}{<} \boldsymbol{\lambda}_0, B(V) {>_Q} = (G, V)_0 \quad \forall\, V \in \mathcal{U} \\ {}_{\mathcal{M}}{<} \boldsymbol{\mu}, B(U_0) {>_Q} = 0 \quad \forall\, \boldsymbol{\mu} \in \mathcal{M}. \end{cases} \tag{2.33}$$

Moreover, $\boldsymbol{\theta}_0 = \nabla w_0$ and w_0 is the solution of the (Kirchhoff-like) problem

$$\Delta^2 w_0 = g \text{ in } \Omega, \qquad w_0 = 0 \text{ and } \frac{\partial w_0}{\partial n} = 0 \text{ on } \partial\Omega. \tag{2.34}$$

□

It is immediate to see that, introducing the linear space

$$\mathcal{Z} = \{V = (v, \boldsymbol{\eta}) \in \mathcal{U} \text{ such that } \boldsymbol{\eta} = \nabla v\}, \tag{2.35}$$

problem (2.33) is equivalent to

$$\begin{cases} \text{Find } U_0 \in \mathcal{Z} \text{ such that} \\ \mathcal{A}_b(U_0, V) = (G, V)_0 \quad \forall\, V \in \mathcal{Z} \end{cases} \tag{2.36}$$

in the sense that: if $(U_0, \boldsymbol{\lambda}_0)$ solves (2.33) then U_0 solves (2.36).

We shall focus on this limit problem in our convergence analysis of the MITC9 shell element. This analysis is tractable and will give a strong indication on whether the element is shear-locking or not when solving this problem using the specified uniform decompositions.

Figures 2.1 and 2.2 give the profiles of the transverse displacement of the plate along its midline, as calculated using the MITC4 shell element – which is in this solution

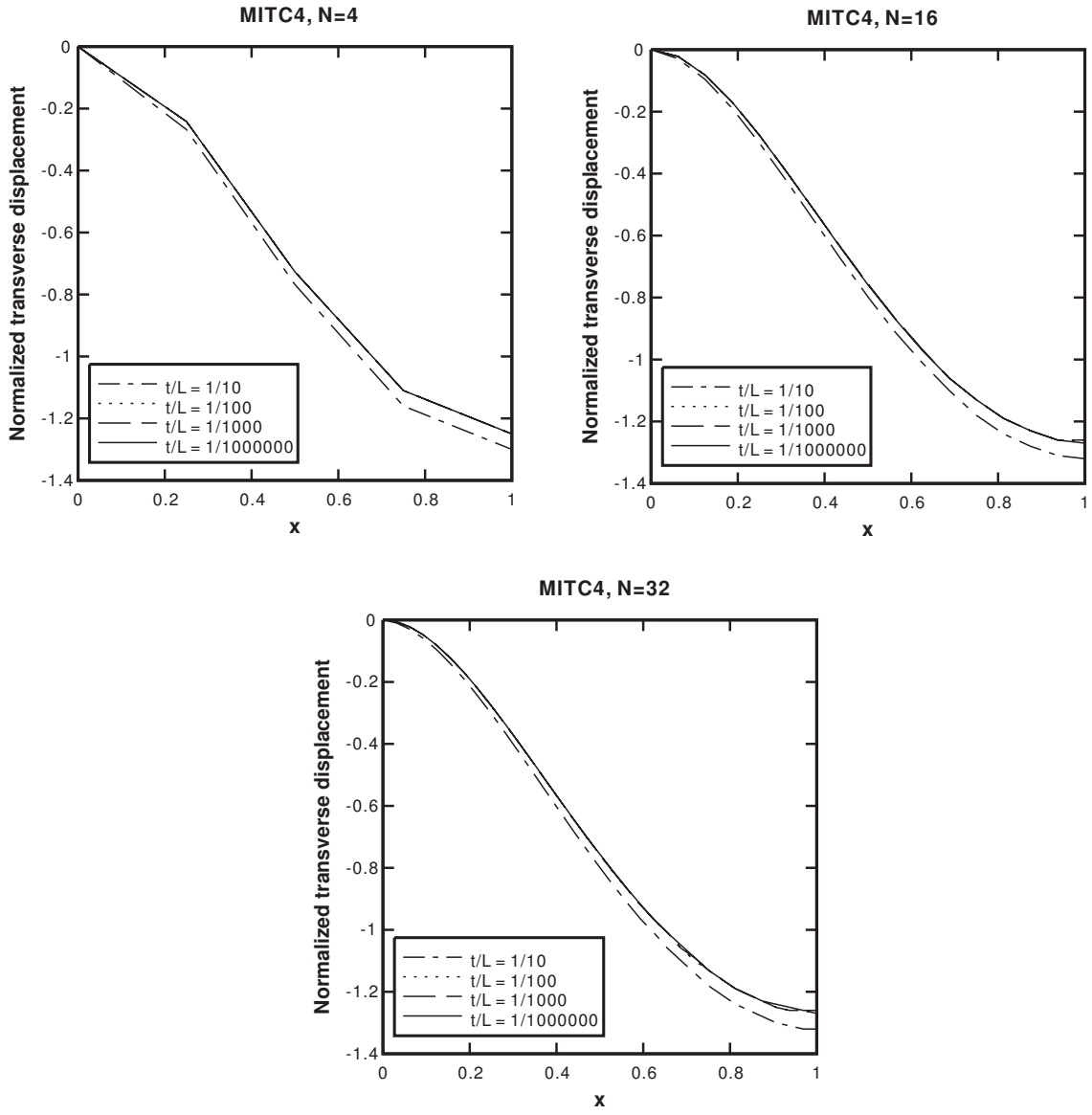

Figure 2.1: The displacement along the mid-line of the plate of Fig. 1.1 is shown for N=4, 16, 32 and different values of plate thickness for the MITC4 element; the normalizing factor is $q/(10^8 * t^3)$. For t/L smaller than 1/100 the displacements are practically equal to those of the case $t/L = 1/100$.

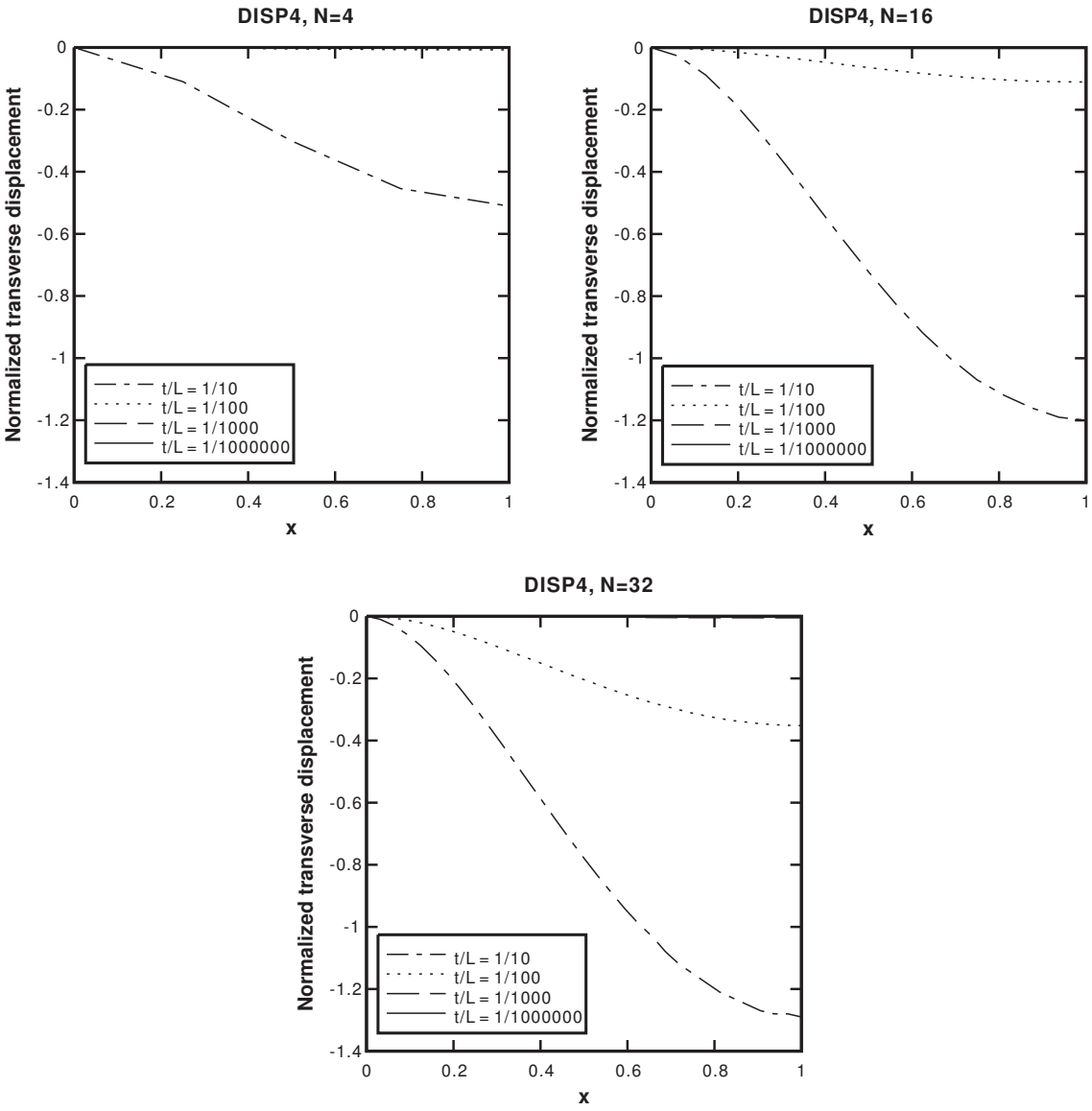

Figure 2.2: The displacement along the mid-line of the plate of Fig. 1.1 is shown for N=4,16,32 and different values of plate thickness for the 4-node displacement-based element, here referred to as DISP4; the normalizing factor is $q/(10^8 * t^3)$. For t/L smaller than 1/100 the displacements are extremely small.

identical to the MITC4 plate element and known to be locking-free [24]– and the 4-node displacement-based element – which is known to severely lock. We see that for the MITC4 shell element, the displacements are indistinguishable for the coarse and fine meshes used when t/L = 1/100 and smaller. Shear deformations contribute to the response when the plate is thick. On the other hand, for the displacement-based element, the displacements become rapidly small when the thickness of the plate decreases, that is, the element locks. These numerical results, together with those of Figure 1.2, illustrate that - as expected - in a mathematical analysis it is reasonable to consider the limit problem as a valuable indicator of the performances of an element for thin and moderately thick plates.

3 The discretized problem

We consider now, for simplicity, a sequence of decompositions $\mathcal{T}_h$ of our domain Ω into rectangles K by means of the points

$$0 \equiv x_0 < x_1 < ... < x_I \equiv L_1 \qquad 0 \equiv y_0 < y_1 < ... < y_J \equiv L_2 \tag{3.1}$$

and we set as usual

$$h_x := \max_{0\le i\le I-1}(x_{i+1} - x_i) \quad h_y := \max_{0\le j\le J-1}(y_{j+1} - y_j) \quad h := \max\{h_x, h_y\}. \tag{3.2}$$

For r and s integers ≥ 0 we define the space $\mathbb{Q}_{r,s}$ as the space of polynomials of degree $\leq r$ in x_1 and of degree $\leq s$ in x_2. When $r = s$ we will just, as usual, write $\mathbb{Q}_r$ instead of $\mathbb{Q}_{r,r}$. Then we consider the finite element spaces

$$\boldsymbol{\Theta}^h := \{\boldsymbol{\theta} \in \boldsymbol{\Theta} \text{ such that } \forall\, K \in \mathcal{T}_h,\ \ \boldsymbol{\theta} \in \mathbb{Q}_2(K)\}, \tag{3.3}$$

$$W^h := \{v \in W \text{ such that } \forall\, K \in \mathcal{T}_h,\ \ v \in \mathbb{Q}_2(K)\}, \tag{3.4}$$

and

$$\mathcal{M}^h := \{\boldsymbol{\mu} \text{ such that } \boldsymbol{\mu}_{|K} \in \mathbb{Q}_{1,2} \times \mathbb{Q}_{2,1}\, \forall\, K \in \mathcal{T}_h\}. \tag{3.5}$$

Finally, we define the reduction operator Π from $(C^0(\overline{\Omega}))^2$ to $\mathcal{M}^h$. For this, on every interval (x_i, x_{i+1}) we define the midpoint x_i^m and the two zeroes of the second degree Legendre polynomial $x_i^{\ell 1}$ and $x_i^{\ell 2}$; similarly, for every interval (y_j, y_{j+1}) we define the midpoint y_j^m and the two zeroes of the second degree Legendre polynomial $y_j^{\ell 1}$ and $y_j^{\ell 2}$ (see Fig. 3.1). Then, for every $\boldsymbol{\chi} \in (C^0(\overline{\Omega}))^2$ we define $\Pi\boldsymbol{\chi}$ as the unique $\boldsymbol{\mu} \in \mathcal{M}^h$ such

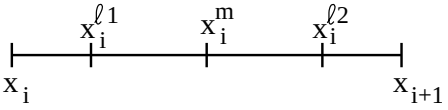

Figure 3.1: Midpoint and two Gauss points for 2-point integration on an interval.

that (see Fig. 3.2)

$$\begin{aligned}
\mu_1(x_i^{\ell 1}, y_j) &= \chi_1(x_i^{\ell 1}, y_j) \qquad i = 0, ..., I-1, \qquad j = 0, ..., J \\
\mu_1(x_i^{\ell 2}, y_j) &= \chi_1(x_i^{\ell 2}, y_j) \qquad i = 0, ..., I-1, \qquad j = 0, ..., J \\
\mu_1(x_i^{\ell 1}, y_j^m) &= \chi_1(x_i^{\ell 1}, y_j^m) \qquad i = 0, ..., I-1, \qquad j = 0, ..., J-1 \\
\mu_1(x_i^{\ell 2}, y_j^m) &= \chi_1(x_i^{\ell 2}, y_j^m) \qquad i = 0, ..., I-1, \qquad j = 0, ..., J-1
\end{aligned} \tag{3.6}$$

and

$$\begin{aligned}
\mu_2(x_i, y_j^{\ell 1}) &= \chi_2(x_i, y_j^{\ell 1}) \qquad i = 0, ..., I, \qquad j = 0, ...J-1 \\
\mu_2(x_i, y_j^{\ell 2}) &= \chi_2(x_i, y_j^{\ell 2}) \qquad i = 0, ..., I, \qquad j = 0, ...J-1 \\
\mu_2(x_i^m, y_j^{\ell 1}) &= \chi_2(x_i^m, y_j^{\ell 1}) \qquad i = 0, ..., I-1, \qquad j = 0, ...J-1 \\
\mu_2(x_i^m, y_j^{\ell 2}) &= \chi_2(x_i^m, y_j^{\ell 2}) \qquad i = 0, ..., I-1, \qquad j = 0, ...J-1
\end{aligned} \tag{3.7}$$

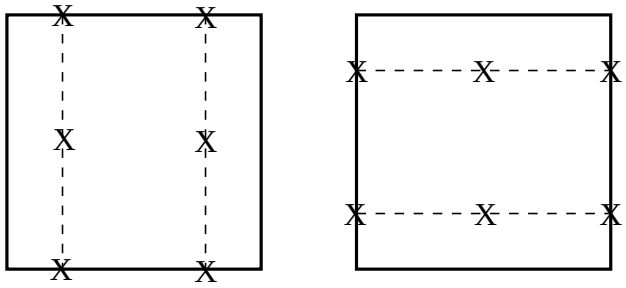

Figure 3.2: D.o.f. for μ_1 (left) and μ_2 (right)

It is important to note that for every $v \in W^h$ we have $\nabla v \in \mathcal{M}^h$, so that

$$\Pi(\nabla v) = \nabla v \qquad \forall v \in W^h. \tag{3.8}$$

Moreover, owing to the (obvious) continuity of Π in finite dimensional spaces made of piecewise smooth functions we easily have

$$\|\Pi \boldsymbol{\eta}\|_0 \lesssim \|\boldsymbol{\eta}\|_0 \qquad \forall \boldsymbol{\eta} \in \boldsymbol{\Theta}^h \tag{3.9}$$

We can now set $\mathcal{U}^h := \boldsymbol{\Theta}^h \times W^h$ and consider the discrete problem:

$$\begin{cases} \text{Find } U^h \equiv (\boldsymbol{\theta}^h, w^h) \in \mathcal{U}^h, \text{ and } \boldsymbol{\lambda}^h \in \mathcal{M}^h \text{ such that} \\ \mathcal{A}_b(U^h, V) + (\boldsymbol{\lambda}^h, \Pi(B(V)))_0 = (G, V)_0 \quad \forall V \in \mathcal{U}^h \\ (\boldsymbol{\mu}, \Pi(B(U^h)))_0 - \dfrac{t^2}{6}(\boldsymbol{\lambda}^h, \boldsymbol{\mu})_0 = 0 \quad \forall \boldsymbol{\mu} \in \mathcal{M}^h. \end{cases} \tag{3.10}$$

Existence and uniqueness of the solution of the discrete problem for $t > 0$ follow exactly as for the continuous problem.

Remark 3.1. *The corresponding* MITC9-plate *element uses the same space* $\boldsymbol{\Theta}^h$ *as in* (3.3)*, while* W_h *consists of local 8-node serendipity functions. The space* $\mathcal{M}$ *is more sophisticated: the first component is made of local* $\mathbb{P}_2$ *polynomials without the monomial* x^2*, while the second component is made of local* $\mathbb{P}_2$ *polynomials without the monomial* y^2 *[6]. The analysis (see e.g. [26]) is largely based on the properties of the* $\mathbb{Q}_2 - \mathbb{P}_1$ *Stokes element. The operator* Π *uses, for each component, the average over the element domain instead of the two internal stations shown in Figure 3.2.*

We now consider and analyze the **limit problem** of (3.10) for $t \to 0$. Introducing the subspace

$$\mathcal{Z}^h = \{V = (v, \boldsymbol{\eta}) \in \mathcal{U}^h \text{ such that } \Pi(\boldsymbol{\eta}) = \nabla v\}, \tag{3.11}$$

it is immediate to see that, for $t \to 0$, $U^h(t)$ converges to the solution U_0^h of the limit problem

$$\begin{cases} \text{Find } U_0^h \in \mathcal{Z}^h \text{ such that} \\ \mathcal{A}_b(U_0^h, V) = (G, V)_0 \quad \forall\, V \in \mathcal{Z}^h, \end{cases} \tag{3.12}$$

that can be obviously seen as a discretization of the continuous limit problem (2.36). Existence and uniqueness of the solution of (3.12) follow immediately from (2.10). Here we want to study the error $\|U_0 - U_0^h\|_{\mathcal{U}}$.

We start with the following "abstract" result.

Theorem 3.2. *Let* $(U_0, \boldsymbol{\lambda}_0)$ *be the solution of* (2.33)*, and let* U_0^h *be the solution of* (3.12)*. Let moreover* U^I *be any element of* $\mathcal{Z}^h$*. Then we have*

$$\|U_0 - U_0^h\|_{\mathcal{U}} \lesssim \|U_0 - U^I\|_{\mathcal{U}} + \sup_{V^h \in \mathcal{Z}^h} \frac{(\boldsymbol{\lambda}_0, B(V^h) - \Pi(B(V^h)))}{\|V^h\|_{\mathcal{U}}}. \tag{3.13}$$

□

Proof. For all $V = (\boldsymbol{\eta}, v) \in \mathcal{Z}^h$ we have first, using (2.10)

$$\|\boldsymbol{\eta}\|_{1,\Omega}^2 \lesssim (\boldsymbol{\varepsilon}(\boldsymbol{\eta}), \boldsymbol{\varepsilon}(\boldsymbol{\eta})) \lesssim \mathcal{A}_b(V, V), \tag{3.14}$$

and using (3.11), (3.9), and (3.14):

$$|\nabla v|_{0,\Omega}^2 = \|\Pi(\boldsymbol{\eta})\|_{0,\Omega}^2 \lesssim \|\boldsymbol{\eta}\|_{0,\Omega}^2 \lesssim \mathcal{A}_b(V, V), \tag{3.15}$$

so that

$$\|V\|_{\mathcal{U}}^2 \lesssim \mathcal{A}_b(V, V) \qquad \forall V \in \mathcal{Z}^h. \tag{3.16}$$

Now we apply (3.16) to $V = U_0^h - U^I$, then we add and subtract U_0, then we use (3.12) and (2.33) for the first term, and the Cauchy-Schwarz inequality for the second:

$$\begin{aligned} \|U_0^h - U^I\|_{\mathcal{U}}^2 &\lesssim \mathcal{A}_b(U_0^h - U^I, U_0^h - U^I) = \mathcal{A}_b(U_0^h - U_0, U_0^h - U^I) + \mathcal{A}_b(U_0 - U^I, U_0^h - U^I) \\ &\lesssim (G, U_0^h - U^I) - \{(G, U_0^h - U^I) - (\boldsymbol{\lambda}_0, B(U_0^h - U^I))\} + \|U_0 - U^I\|_{\mathcal{U}} \|U_0^h - U^I\|_{\mathcal{U}} \\ &= (\boldsymbol{\lambda}_0, B(U_0^h - U^I)) + \|U_0 - U^I\|_{\mathcal{U}} \|U_0^h - U^I\|_{\mathcal{U}}. \end{aligned} \tag{3.17}$$

To treat the first term in the last line of (3.17) we remember that $\Pi(B(U_0^h - U^I)) = 0$ so that

$$\begin{aligned} |(\boldsymbol{\lambda}_0, B(U_0^h - U^I))| &= |(\boldsymbol{\lambda}_0, B(U_0^h - U^I) - \Pi(B(U_0^h - U^I)))| \\ &\le \Big(\sup_{V^h \in \mathcal{Z}^h} \frac{(\boldsymbol{\lambda}_0, B(V^h) - \Pi(B(V^h)))}{\|V^h\|_{\mathcal{U}}} \Big) \|U_0^h - U^I\|_{\mathcal{U}}. \end{aligned} \tag{3.18}$$

Inserting (3.18) in (3.17) and simplifying by $\|U_0^h - U^I\|_{\mathcal{U}}$ we get the result. □

4 Error estimates for the limit problem

Here we want to apply the general result of Theorem 3.2 to our specific discretization. To this purpose we need an estimate for the two pieces appearing on the right-hand side of (3.13). We start with the first one.

Theorem 4.1. *Let $(U_0, \boldsymbol{\lambda}_0) \equiv ((\boldsymbol{\theta}_0, w_0), \boldsymbol{\lambda}_0)$ be the solution of (2.33). Then there exist $\boldsymbol{\theta}^I \in \boldsymbol{\Theta}^h$ and $w^I \in W^h$ such that*

$$\|\boldsymbol{\theta}_0 - \boldsymbol{\theta}^I\|_{1,\Omega} \le C\, h^2\, \|w_0\|_{4,\Omega}, \tag{4.1}$$

$$\|w_0 - w^I\|_{1,\Omega} \le C\, h^2\, \|w_0\|_{3,\Omega}, \tag{4.2}$$

$$\Pi \boldsymbol{\theta}^I = \nabla w^I. \tag{4.3}$$

Proof. We follow techniques similar to those used in [27]. Define first $\widetilde{w}$ as the Bogner-Fox-Schmit approximation of w_0 defined locally by:

$$\begin{aligned} &\widetilde{w} \in C^1(\Omega): \quad \widetilde{w}_{|K} \in \mathbb{Q}_3(K) \quad \forall K, \\ &\widetilde{w} = w_0,\ \widetilde{w}_x = (w_0)_x,\ \widetilde{w}_y = (w_0)_y,\ \widetilde{w}_{xy} = (w_0)_{xy} \text{ at the vertices of each } K, \end{aligned} \tag{4.4}$$

and recall that, on each K,

$$|\widetilde{w} - w_0|_{s,K} \leq C\, h^{r-s} |w_0|_{r,K}, \qquad 0 \leq s \leq r \leq 4. \tag{4.5}$$

Next, let $\widetilde{w}^I \in W_h$ be the *classical 9-nodes continuous interpolant* of $\widetilde{w}$, defined locally by

$$\begin{aligned} &\widetilde{w}^I \in \mathbb{Q}_2(K) \quad \forall K, \\ &\widetilde{w}^I = \widetilde{w} \text{ at the four vertices of each element } K, \\ &\widetilde{w}^I = \widetilde{w} \text{ at the midpoints of each edge } e \text{ of } K, \quad \forall K, \\ &\widetilde{w}^I = \widetilde{w} \text{ at the barycenter of each element } K, \end{aligned} \tag{4.6}$$

for which the following estimate holds

$$|\widetilde{w} - \widetilde{w}^I|_{s,K} \leq C\, h^{r-s} |\widetilde{w}|_{r,K} \leq C\, h^{r-s} |w_0|_{r,K}, \qquad 0 \leq s \leq r \leq 3 \tag{4.7}$$

for all K. Setting $w^I = \widetilde{w}^I$, from (4.5) and (4.7) we have then in particular

$$\|w_0 - w^I\|_{1,\Omega} \leq \|w_0 - \widetilde{w}\|_{1,\Omega} + \|\widetilde{w} - w^I\|_{1,\Omega} \leq C\, h^2 |w_0|_{3,\Omega}. \tag{4.8}$$

We notice that an alternative, equivalent definition of (4.6) is:

$$\begin{aligned} &\widetilde{w}^I \in \mathbb{Q}_2(K) \quad \forall K, \\ &\widetilde{w}^I = \widetilde{w} \text{ at the four vertices of each element } K, \\ &\int_e (\widetilde{w} - \widetilde{w}^I) ds = 0 \text{ on each edge } e \text{ of } K, \quad \forall K, \\ &\int_K (\widetilde{w} - \widetilde{w}^I) dx dy = 0, \quad \forall K. \end{aligned} \tag{4.9}$$

Indeed, by Simpson integration formula on each edge, exact for polynomials of degree ≤ 3 we deduce

$$\int_e (\widetilde{w} - \widetilde{w}^I) ds = 0 \text{ on each edge } e \text{ of } K.$$

By applying tensor-product Simpson rule we also deduce

$$\int_K (\widetilde{w} - \widetilde{w}^I) dxdy = 0 \quad \forall K.$$

We define now $\boldsymbol{\theta}^I \in \boldsymbol{\Theta}^h$ as the *continuous interpolant* of $\nabla\widetilde{w}$ defined as in (4.6), that is,

$$\theta_1^I = \widetilde{w}_x, \quad \theta_2^I = \widetilde{w}_y \text{ at the 9 nodes.} \tag{4.10}$$

From (4.5) and (4.7) we deduce

$$\|\boldsymbol{\theta}_0 - \boldsymbol{\theta}^I\|_{1,\Omega} = \|\nabla(w_0 - \widetilde{w}) + \nabla\widetilde{w} - \boldsymbol{\theta}^I\|_{1,\Omega} \leq C\, h^2 |w_0|_{4,\Omega}. \tag{4.11}$$

In order to prove (4.3), let $K \equiv (x_i, x_{i+1}) \times (y_j, y_{j+1})$ be an element of $\mathcal{T}_h$, let $e(x, y_j) := \widetilde{w}(x, y_j) - \widetilde{w}^I(x, y_j)$, and let $p_1(x)$ be any polynomial of degree ≤ 1. Using (4.6) and (4.9) we easily have that $e(x, y_j)$ vanishes at the endpoints and it has zero mean value on (x_i, x_{i+1}). Hence, integrating by parts,

$$\int_{x_i}^{x_{i+1}} e_x(x, y_j) p_1(x)\, \mathrm{d}x = -\int_{x_i}^{x_{i+1}} e(x, y_j) p_{1,x}(x)\, \mathrm{d}x + e(x, y_j) p_1(x)\Big|_{x_i}^{x_{i+1}} = 0.$$

It follows then that $e_x(x, y_j)$ is a Legendre polynomial of degree 2. As such, it vanishes at the 2 Gauss points $x_i^{\ell 1},\ x_i^{\ell 2}$ of (x_i, x_{i+1}). Hence,

$$\widetilde{w}_x(x_i^{\ell 1}, y_j) = \widetilde{w}_x^I(x_i^{\ell 1}, y_j), \quad \widetilde{w}_x(x_i^{\ell 2}, y_j) = \widetilde{w}_x^I(x_i^{\ell 2}, y_j). \tag{4.12}$$

We further remark that on the horizontal line $y = y_j$ we have that θ_1^I and $\widetilde{w}_x$ are both polynomial of degree 2. Using (4.10) we see that they coincide at three points, and hence they coincide on the whole line. Hence we might rewrite (4.12) as

$$\theta_1^I(x_i^{\ell 1}, y_j) = \widetilde{w}_x^I(x_i^{\ell 1}, y_j), \quad \theta_1^I(x_i^{\ell 2}, y_j) = \widetilde{w}_x^I(x_i^{\ell 2}, y_j). \tag{4.13}$$

With the same argument we deduce that $\theta_1^I(x, y) - \widetilde{w}_x^I(x, y)$ also vanishes at the Gauss points of $y = y_{j+1}$ and $y = y_j^m$. For θ_2^I the same argument applies on the vertical edges, using $e_y(x_i, y) = \widetilde{w}_y(x_i, y) - \widetilde{w}_y^I(x_i, y)$, so that

$$\Pi\boldsymbol{\theta}^I = \nabla\widetilde{w}^I, \tag{4.14}$$

and the proof is concluded. □

Remark 4.2. *The construction of $\boldsymbol{\theta}^I$ and w^I (crucial for establishing the final estimates) could have been made also by more traditional techniques (i.e., through the "Stokes + Raviart-Thomas" approach). This however would have required the use of the $\mathbb{Q}_2 - \mathbb{Q}_1$ Stokes element. The analysis of this element is not simple, and in general requires restrictions on the geometry of the elements (see [28]). Therefore we prefer the present construction because the extension to more general situations seems to have more possibilities.*

In order to estimate the second piece of the right-hand side of (3.13) we make first two crucial observations.

The first one, quite obvious, is that Π coincides with the identity operator when applied to constant vectors. For every $\boldsymbol{\eta} \in \boldsymbol{\Theta}^h$ we can then denote by $\overline{\boldsymbol{\eta}}$ its piecewise L^2 projection on constant vectors, and adding and subtracting $\overline{\boldsymbol{\eta}} \equiv \Pi\overline{\boldsymbol{\eta}}$, and using (3.9) and usual approximation results we have

$$\|\boldsymbol{\eta} - \Pi\boldsymbol{\eta}\|_0 = \|(\boldsymbol{\eta} - \overline{\boldsymbol{\eta}}) + \Pi(\overline{\boldsymbol{\eta}} - \boldsymbol{\eta})\|_0 \leq \|(\boldsymbol{\eta} - \overline{\boldsymbol{\eta}})\|_0 + \|\Pi(\overline{\boldsymbol{\eta}} - \boldsymbol{\eta})\|_0 \lesssim h\|\boldsymbol{\eta}\|_1. \tag{4.15}$$

The second observation is that for every $\boldsymbol{\eta} \in \boldsymbol{\Theta}^h$ and for every $K \in \mathcal{T}_h$ the first component η_1 is a polynomial in $\mathbb{Q}_2$ while $(\Pi\boldsymbol{\eta})_1$ is a polynomial of $\mathbb{Q}_{1,2}$ that coincides with η_1 at the two Legendre points of the horizontal lines $y = y_j$, $y = y_{j+1}$ and $y = y_j^m$. Hence, on each of the vertical lines $x = x_i^{\ell 1}$ and $x = x_i^{\ell 2}$ the two polynomials η_1 and $(\Pi\boldsymbol{\eta})_1$ (as polynomials of degree two that coincide at three different points) coincide on the whole line. Consequently, by applying two-point Gauss integration in x, and Simpson's rule in y, we immediately see that

$$\int_K \eta_1(x,y) - (\Pi\boldsymbol{\eta})_1(x,y)\,\mathrm{d}x\,\mathrm{d}y = \int_{y_j}^{y_{j+1}} \mathrm{d}y \int_{x_i}^{x_{i+1}} \eta_1(x,y) - (\Pi\boldsymbol{\eta})_1(x,y)\,\mathrm{d}x = 0.$$

The same arguments obviously apply to the second component, so that we can write

$$\int_K \boldsymbol{\eta}(x,y) - (\Pi\boldsymbol{\eta})(x,y)\,\mathrm{d}x\,\mathrm{d}y = 0. \tag{4.16}$$

We can now easily estimate the second term of (3.13).

Theorem 4.3. *Let $(U_0, \boldsymbol{\lambda}_0) \equiv ((\boldsymbol{\theta}_0, w_0), \boldsymbol{\lambda}_0)$ be the solution of (2.33). Then for every $V^h = (v, \boldsymbol{\eta}) \in \mathcal{U}^h$ we have*

$$|(\boldsymbol{\lambda}_0, B(V^h) - \Pi(B(V^h)))_0| \lesssim h^2 \|\boldsymbol{\lambda}_0\|_{1,\Omega}\, \|V^h\|_{\mathcal{U}}. \tag{4.17}$$

Proof. We begin by recalling that from (2.24) we have $B(V^h) = \nabla v - \boldsymbol{\eta}$, and from (3.8) we have $\Pi(\nabla v) = \nabla v$, so that

$$B(V^h) - \Pi(B(V^h)) = -\boldsymbol{\eta} + \Pi(\boldsymbol{\eta}). \tag{4.18}$$

Hence, introducing $\overline{\boldsymbol{\lambda}_0}$ as the piecewise constant mean value of $\boldsymbol{\lambda}_0$, using (4.16)and Cauchy-Schwarz, and then usual approximation results and (4.15) we have

$$\begin{aligned}\Big| \int_\Omega \boldsymbol{\lambda}_0(\boldsymbol{\eta} - \Pi\boldsymbol{\eta})\,\mathrm{d}x\,\mathrm{d}y\Big| = \\ \Big| \int_\Omega (\boldsymbol{\lambda}_0 - \overline{\boldsymbol{\lambda}_0})(\boldsymbol{\eta} - \Pi\boldsymbol{\eta})\,\mathrm{d}x\,\mathrm{d}y\Big| &\le \|\boldsymbol{\lambda}_0 - \overline{\boldsymbol{\lambda}_0}\|_{0,\Omega}\,\|\boldsymbol{\eta} - \Pi\boldsymbol{\eta}\|_{0,\Omega} \\ &\lesssim h^2\|\boldsymbol{\lambda}_0\|_{1,\Omega}\,\|\boldsymbol{\eta}\|_{1,\Omega}. \end{aligned} \tag{4.19}$$

□

Collecting the result of Theorem 3.2 together with the results of Theorems 4.1 and 4.3 we now have the final result.

Theorem 4.4. *Let* $(U_0, \boldsymbol{\lambda}_0) \equiv ((w_0, \boldsymbol{\theta}_0), \boldsymbol{\lambda}_0)$ *be the solution of* (2.33)*, and let* U_0^h *be the solution of* (3.12)*. Then we have*

$$\|U_0 - U_0^h\|_{\mathcal{U}} \lesssim h^2\,(\|w_0\|_{3,\Omega} + \|\boldsymbol{\lambda}_0\|_{1,\Omega}). \tag{4.20}$$

Therefore the element should behave optimally in the numerical plate solution considered in Fig. 1.1 and this is indeed the case as shown in Fig. 1.2 .

5 Concluding remarks

Our objective in this paper was to give a mathematical analysis of the MITC9 shell element when used in plate bending solutions. Shell elements are used in general to model plate structures in engineering and the sciences; hence the analysis pursued herein is of considerable interest. While we considered a simplified setting, namely a clamped plate problem solved using uniform meshes and the *limit problem* with plate thickness equal to zero, the analysis is valuable because it gives insight into the behavior of the element.

The mathematical convergence analysis given in the paper shows that in this simple setting the element behaves optimally for displacements and rotations and hence does not lock. Some numerical results given in the paper also illustrate that it is reasonable to consider the case of vanishing plate thickness for the mathematical analysis.

Considering future work, since we used in all our analyses uniform meshes, it would be of value to also study the performance of the element in non-uniform decompositions, as well as the case of positive thickness. Furthermore, a more general mathematical convergence analysis of the MITC9 shell element when used for the solution of actual shell problems, that is, involving curved thin structures, would be very valuable.

References

[1] Bathe KJ. Finite element procedures. New York: Prentice Hall; 1996.

[2] Zienkiewicz OC. and Taylor RL, The finite element method. Butterworth-Heinemann; 2005.

[3] Brezzi F, Bathe KJ, and Fortin M, Mixed-interpolated elements for Reissner/Mindlin plates, Int. J. Num. Methods in Engineering, 28, 1787-1801, 1989.

[4] Brezzi F and Fortin M. Mixed and hybrid finite element methods. Springer; 1991.

[5] Bathe KJ, Brezzi F, and Cho SW. The MITC7 and MITC9 plate bending elements. Comput Struct 1989;32:797-814.

[6] Bathe KJ, Bucalem M, and BrezziF. Displacement and stress convergence of the MITC plate bending elements, J. Eng. Computations, 7, no. 4, 291-302, 1990.

[7] Chapelle D and Bathe KJ. Fundamental considerations for the finite element analysis of shell structures. Comput Struct 1998;66:19-36,711-2.

[8] Chapelle D and Bathe KJ. The finite element analysis of shells - Fundamentals. Springer; 2003, 2nd edition in press.

[9] Lee PS and Bathe KJ. On the asymptotic behavior of shell structures and the evaluation in finite element solutions. Comput Struct 2002;80:235-55.

[10] Lee PS and Bathe KJ. Insight into finite element shell discretizations by use of the basic shell mathematical model. Comput Struct 2005;83:69-90.

[11] Blouza A, Brezzi F, and Lovadina C. On the classification of linearly elastic shells C.R.A.S., Série I 1991;328:831-836

[12] Baiocchi C and Lovadina C. A shell classification by interpolation. Mat. Mod. Methods Appl. Sci. 2002;12:1359-1380

[13] Beirão da Veiga L. Asymptotic energy behavior of two classical intermediate benchmark shell problems. Mat. Mod. Methods Appl. Sci. 2003;13:1279-1302

[14] Beirão da Veiga L and Chinosi C. Numerical evaluation of the asymptotic energy behavior of intermediate shells with application to two classical benchmark tests. Comput Struct 2004;82:525-34.

[15] Beirão da Veiga L. Asymptotic study of the solution for pinched cylindrical shells Comp. Meth. Appl. Mech. Engrg. 2005;194: 1113-39

[16] Hiller JF and Bathe KJ. Measuring convergence of mixed finite element discretizations: An application to shell structures. Comput Struct 2003;81:639-54.

[17] Bathe KJ and Lee PS. Measuring the convergence behavior of shell analysis schemes, Comput Struct, in press.

[18] Kardestuncer H.(ed), Finite element handbook, MacGraw-Hill, 1987.

[19] Bucalem M and Bathe KJ. The mechanics of solids and structures - hierarchical modeling and the finite element solution, Springer, to appear.

[20] Bathe KJ. The finite element method, in Encyclopedia of Computer Science and Engineering, B. Wah (ed.), J. Wiley and Sons; 2009, 1253-64.

[21] Lee PS, Bathe KJ. The quadratic MITC plate and MITC shell elements in plate bending. Advances in Engineering Software 2010;41:712-28.

[22] Bathe KJ, Lee PS, Hiller JF. Towards improving the MITC9 shell element. Comput Struct 2003;81:477-89.

[23] Bucalem M and Bathe KJ. Higher-order MITC general shell elements, Int. J. for Numerical Methods in Engineering, 36, 3729-3754, 1993.

[24] Iosilevich A, Bathe KJ, and Brezzi F. On evaluating the inf-sup condition for plate bending elements, Int. Journal for Numerical Methods in Engineering, 40, 3639-3663, 1997.

[25] Chapelle D and Bathe KJ. On the ellipticity condition for model-parameter dependent mixed formulations, Comput Struct 2010; 88:581-87.

[26] Brezzi F, Fortin M, Stenberg R Error Analysis of mixed-interpolated elements for Reissner-Mindlin plates, Math. Mod. and Meth. in Appl. Sci. M3 AS, 1, 125-151, 1991.

[27] Brezzi F, Evans JA, Hughes TJR, and Marini LD. New Quadrilateral Plate Elements Based on Twist-Kirchhoff Theory, in preparation.

[28] Stenberg R. Blandade finita elementmetoder för två problem inom strömningsmekaniken och hållfathetsläran, Licentiatarbete, Department of Technical Physics and Mathematics, Helsinki University of Technology, 1981.